

Star formation in LINER host galaxies at $z \sim 0.3$

Silvia Tommasin¹, Hagai Netzer¹, Amiel Sternberg¹
School of Physics and Astronomy, Tel Aviv University, Tel Aviv 69978, Israel
 and

Raanan Nordon², Dieter Lutz²
MPE, Postfach 1312, 85741, Garching, Germany

Angela Bongiorno³
INAF-Osservatorio Astronomico di Roma, via Frascati 33, 00040 Monte Porzio Catone (Roma), Italy

Stefano Berta², Benjamin Magnelli²

Emeric Le Floch⁴, Laurie Riguccini⁴
*Laboratoire AIM, CEA/DSM-CNRS-Universit  Paris Diderot, IRFU/Service d'Astrophysique, Bt.709,
 CEA-Saclay, 91191 Gif-sur-Yvette Cedex, France*

Francesca Pozzi⁵
Dipartimento di Astronomia, Universit  degli Studi di Bologna, via Ranzani 1, 40127 Bologna, Italy

ABSTRACT

We present the results of a *Herschel*-PACS study of a sample of 97 LINERs at redshift $z \sim 0.3$ selected from the zCOSMOS survey. Of these sources, 34 are detected in a least one PACS band, enabling reliable estimates of the far-infrared L_{FIR} luminosities, and a comparison to the FIR luminosities of local LINERs. Many of our PACS-detected LINERs are also UV sources detected by *Galex*. Assuming that the FIR is produced in young dusty star-forming regions, the typical star-formation rates (SFRs) for the host galaxies in our sample is $\sim 10 M_{\odot} \text{ yr}^{-1}$, 1–2 orders of magnitude larger than in many local LINERs. Given stellar masses inferred from optical/NIR photometry of the (unobscured) evolved stellar populations, we find that the entire sample lies close to the star-forming “main sequence” for galaxies at redshift 0.3. For young star-forming regions, the $H\alpha$ - and UV-based estimates of the SFRs are much smaller than the FIR-based estimates, by factors ~ 30 , even assuming that all of the $H\alpha$ emission is produced by O-star ionization rather than by the AGNs. These discrepancies may be due to large (and uncertain) extinctions towards the young stellar systems. Alternatively, the $H\alpha$ and UV emissions could be tracing residual star-formation in an older less obscured population with decaying star formation. We also compare L_{SF} and $L(\text{AGN})$ in local LINERs and in our sample and comment on the problematic use of several line diagnostic diagrams in cases similar to the sample under study.

Subject headings: LINER; AGN; SFR

1. Introduction

Galaxies containing Low Ionization Nuclear Emission-line Regions (LINERs) are characterized by optical emission lines including $[OIII]\lambda 5007$, $[OII]\lambda 3727$, $[NII]\lambda 6584$, $[SII]\lambda 6717, 6731$, and hydrogen Balmer lines. All these lines are prominent in active-galactic-nuclei (AGN) but in LINERs the relative intensities indicate a low ionization state (e.g. Heckman 1980; Ho 2008). The lower level of ionization compared with Seyfert 2 galaxies for example (hereafter “high ionization type-II AGNs”) manifests itself in several ways, such as by the $[OIII]\lambda 5007/H\beta$ line ratio that is 3–5 times smaller in LINERs. In the local universe LINERs are found in about 1/3 of all galaxies brighter than $B_T=15.5$ mag. This is larger than the number of high ionization type-II AGNs by a factor of 10 or more (e.g. Ho et al. 1997). Local high ionization AGN and LINERs are present in galaxies with similar bulge luminosities and sizes, neutral hydrogen gas (H I) contents, optical colors and stellar masses (Ho 2008).

Explanations for the origin of LINERs include shock excitation (e.g. Nagar et al. 2005; Dopita et al. 1997) and photoionization by evolved (pAGB) stellar populations (e.g. Annibali et al. 2010). However, photoionization by a low-luminosity AGN is likely responsible for many if not most LINERs, especially those with relatively bright ($EW > 3\text{\AA}$) $H\alpha$ lines (Ferland & Netzer 1983; Barth et al. 1998; Maoz et al. 2005; Ho 1999; Gonzalez-Martin et al. 2006). Indeed some LINERs show UV continuum variations (Maoz et al. 2005), and spectral energy distributions (SEDs) typical of accretion onto massive black holes (BHs), and contain nuclear hard X-ray sources more luminous than expected for a normal population of X-ray binaries. They also contain compact nuclear radio sources similar to those seen in AGN (e.g. Nagar et al. 2000; Falcke et al. 2000). Various studies (Kewley et al. 2006; Ho 2008; Kauffmann & Heckman 2009; Netzer 2009) show that nuclear excited LINERs and high ionization type-II AGNs form a continuous sequence in normalized accretion rate, L/L_{Edd} , with LINERs at the low end of the sequence.

As for all AGN, LINERs can be classified into type-I (broad emission lines) and type-II (only narrow lines) sources. The broad lines, when ob-

served, are seen almost exclusively in $H\alpha$ but hardly in $H\beta$. This is most likely due the weakness of the broad wings that are difficult to observe against the strong stellar continua. In many cases the classification is ambiguous and the relative number of type-I and type-II LINERs is uncertain even at very low redshift (see Ho 2008).

There have been several recent publications concerning the infrared (IR) properties of LINERs. Sturm et al. (2006) studied 33 LINERs with *Spitzer*. More than half are from the revised Bright galaxy survey (Veilleux et al. 1995) and are hence very bright in the IR with twelve sources showing ULIRG or LIRG luminosities. Their sample includes two different populations of LINERs: IR-faint, with emissions arising mostly in compact nuclear regions, and IR-luminous, which often show spatially extended, non-AGN emissions. The two populations are distinguished by their mid-IR (MIR) continuum SEDs, the luminosities of PAH features, and mid-IR fine structure emission lines. IR-luminous LINERs have MIR SEDs typical of starburst galaxies while the MIR SEDs of IR-faint LINERs are considerably bluer. Strong highly excited $[OIV]$ emissions are detected in both populations, indicative of AGN photoionization. According to Sturm et al. (2006), the two LINER groups occupy different regions of the MIR emission-line excitation diagrams.

Dudik et al. (2009) considered a sample of 67 LINERs observed with *Spitzer* including many of Sturm et al. (2006) objects. They found AGN signatures, such as the $[NeV]14.32, 24.31\mu\text{m}$ line, in 26 sources and concluded that many of the AGN sources in LINERs are heavily obscured, even in the MIR. The fraction of AGN is as high as 74% if all AGN diagnostics (including X-ray) are included. The mean redshift of these sources is small with only some objects at $z > 0.05$. The median IR luminosity (L_{IR}) in this sample is about $10^{43.5}$ erg/sec with eight sources with $L_{IR} > 10^{44.5}$ erg/sec. Some very luminous IR galaxies (ULIRGs with $L_{IR} > 10^{45.6}$ erg/sec) also display LINER-like optical spectra. However, in these sources, the optical emission lines may be produced in shocked gas, rather than by AGN photoionization.

In this paper we present new FIR *Herschel* photometry for a sample of $z \sim 0.3$ optically selected LINERs. A visual inspection of HST images of our sample galaxies show that most of them are late-

type galaxies. Classifying such sources by their emission line spectrum, in particular estimating the contribution to their Balmer lines from SF regions, is not a trivial issue since some emission from H II regions is present in almost all galaxies. This is particularly problematic at intermediate and high redshift where even a narrow slit can cover a large fraction of the host galaxy. Large aperture UV observations of LINER galaxies, such as those commonly provided by *Galex*, can also confuse a nuclear UV continuum source (in the case of type-I LINERs) with more extended UV emission from SF regions in the host galaxy. Also, a redshift of 0.3 is large enough to prevent the detection of a weak nuclear X-ray source typical of nearby LINERs. The primary goal of our paper is to use the FIR measurements to infer the global star-formation rates of the LINER host galaxies.

2. Observations

2.1. Optical observations

The zCOSMOS-bright survey includes about 20,000 galaxies with $0.1 < z < 1.2$ and $i_{AB} < 22.5$ mag. within the 1.7 deg^2 COSMOS ACS field¹ (centered on 10h00m28.6s, +02d12m21s). Objects in this field were observed with the VIMOS spectrograph on the VLT (Lilly et al. 2007) and those discussed here are from the first 10,000 COSMOS objects. Bongiorno et al. (2010) selected 213 type-II AGNs from the sample for which they measured redshifts, line fluxes and equivalent widths after removing the stellar continuum through their automated pipeline (platefit_vimos). They also derived aperture correction factors in the i_{AB} band to take into account the small slit size ($1''$). The objects span the redshift range $0.15 < z < 0.92$ and the luminosity range $10^{5.5} L_{\odot} < L([OIII]\lambda 5007) < 10^{9.1} L_{\odot}$ where $L([OIII]\lambda 5007)$ is the extinction corrected $[OIII]\lambda 5007$ luminosity. Bongiorno et al. (2010) combined their sample with type-II AGNs drawn from the Sloan Digital Sky Survey (SDSS) data release 7 (DR7). The additional sample included 291 objects with $0.3 < z < 0.83$ and $10^{7.3} L_{\odot} < L([OIII]\lambda 5007) < 10^{10.1} L_{\odot}$. Using the combined sample they found that type-II

AGN evolution is well described by a luminosity-dependent density evolution model.

Among the 213 zCOSMOS-bright type-II AGNs, 97 objects are classified as LINERs using standard BPT (Baldwin Phillips & Terlevich 1981) classification based on $[NII]/H\alpha$ and/or $[SII]/H\alpha$ versus $[OIII]/H\beta$. All line fluxes were corrected for reddening based on the observed $H\alpha/H\beta$ line ratio and the galactic extinction law. The requirement to measure $H\alpha$ and the adjacent $[NII]\lambda 6584$ emission line limits the redshift of this group to $z \leq 0.445$. Two of the sources (819596 and 827400) do not have reliable $[NII]\lambda 6584$ measurements and were classified according to $[SII]\lambda 6717, 6731/H\alpha$. The classification is based only on sources with $S/N > 3$ for $[OIII]\lambda 5007$ and $S/N > 2.5$ for the other emission lines. Five of the sources were found to have less reliable line ratios after the publication of Bongiorno et al. (2010). We include these sources and flag them in all tables but not in diagrams because they do not show any peculiar behaviour. The S/N of all observations is too low to search for weak broad $H\alpha$ lines and we consider all our objects to be type-II LINERs.

2.2. *Herschel* observations

The above sample of zCOSMOS LINERs was observed by *Herschel*-PACS as part of the PACS Evolutionary Probe survey (PEP) (Lutz et al. 2011). PEP is a guaranteed-time key program to survey the extragalactic sky with the aim of studying the rest-frame far-IR emission of galaxies up to redshift 3. PEP blank fields include COSMOS, Lockman Hole, E-CDFS, Groth Strip, GOODS-S and GOODS-N². Data processing, map computing and source extraction are described in Berta et al. (2010).

Out of the 97 LINERs in our sample, 34 have $\sigma > 3$ detections in the $100 \mu\text{m}$ and/or the $160 \mu\text{m}$ PACS bands (the 3σ limits are 5 mJy and 11 mJy , respectively; see e.g. PEP COSMOS v. 2.0, October 2010). A search through the archive reveals 5 more SDSS LINERs in the COSMOS field that were detected by *Herschel*. These sources have composite H II/LINER spectra and hence we do not include them in the sample of “pure” LINERs considered here. The positions of the PACS de-

¹<http://irsa.ipac.caltech.edu/data/COSMOS/spectra/z-cosmos/>

²<http://www.mpe.mpg.de/ir/Research/PEP/index.php>

tected LINERs in the BPT diagram are shown in Figure 1.

Of the 34 *Herschel* LINERs, 18 are detected at both $100\mu\text{m}$ and $160\mu\text{m}$, 12 only at $100\mu\text{m}$ and 4 only at $160\mu\text{m}$. The redshift range of these sources is 0.255–0.445. More information is provided in Table 1. The remaining 62 zCosmos LINERs with $\sigma < 3$ are considered non-detections. Among these 62 sources, 40 have optical line S/N > 3 and we stacked them in two subgroups according to the estimated stellar masses of the host galaxies ($M_* \leq 10^{9.5}$, see § 3, we chose this threshold in order to obtain subgroups with a similar number of objects) and found $L_{IR} = 1.68 \pm 0.34 \times 10^{10} L_\odot$ for $M_* > 10^{9.5}$ and $L_{IR} < 0.66 \times 10^{10} L_\odot$ for $M_* < 10^{9.5}$, considering $z \sim 0.3$. This allows us to obtain mean M_* and SFR, under different assumptions, for those sub-samples as described below.

2.3. *Spitzer* observations

We found 13 of the 34 PACS-detected sources to have mid-IR photometric observations by *Spitzer*-IRAC (3.6, 4.5, 5.6, $8.0\mu\text{m}$) and *Spitzer*-MIPS (24, 70, $160\mu\text{m}$). We obtained *Spitzer* photometry for these sources from Kartaltepe et al. (2010) assuming the separation between the optical and MIR positions is less than 4" (the MIPS angular resolution at $70\mu\text{m}$ is about 8").

Besides all the sources, but 818456 and 812330, have been detected at $24\mu\text{m}$ and are included in the S-COSMOS MIPS 24 Photometry Catalog, October 2008.

2.4. *Galex* UV observations

Among the sample of 34 PACS-detected LINERs, 23 have both *Galex* near UV (NUV, peak at 2271\AA) and far UV (FUV, peak at 1528\AA) detections within 2" from the center of the optical images. The angular resolution in the FUV band is $2''.5$ – $3''.5$ and in the NUV band $3''.5$ – $5''$ (Bianchi et al. 1999) and we consider those as real UV detections. Two objects have only FUV detections and 4 only NUV detections. Thus, 85% the PACS-detected LINERs have at least one UV detection. Out of the 62 LINERs that were not detected by PACS, 39 were detected by *Galex* in both bands, 7 only in the FUV band and 10 only in the NUV band i.e., 90% of the PACS non-detected sources have at least one *Galex* detection.

Data for the UV sources were retrieved from the *Galex* archive³ and are given in Table 1. We find that LINERs detected by PACS are marginally brighter in the UV, see Figure 2.

We used the data from the two *Galex* bands to calculate the UV spectral slope, β , assuming $F_\lambda \propto \lambda^\beta$ (see Table 1). This index is considered a good indicator of dust extinction in LIRGs and other SF galaxies at high redshift (e.g. Meurer et al. 1999; Seibert et al. 2005). The *Galex* bands, especially the NUV band, are very broad which affects our estimates of the spectral slopes. For each β we can then estimate the rest-wavelength 1528\AA flux which we then combine with the derived extinction to estimate the UV-based SFR (§ 3).

Meurer et al. (1999), Bouwens et al. (2009), Gallerani et al. (2010) and several others provided empirical relationships between the absorption in the UV (e.g. $A(1600\text{\AA})$) and β . We derived a similar expression for the objects in our sample based on a Calzetti-type extinction law of the form $A_\lambda \propto \lambda^{-0.7}$. This gives,

$$A_{1528} = 3.96 + 1.8\beta \text{ mag.} \quad (1)$$

The extinction corrected UV fluxes and luminosities are discussed in § 3.3.

3. Star formation rates and stellar masses in LINER host galaxies

3.1. Star formation rate calibrations

The primary SFR indicators we are considering in this paper are the far-IR luminosity $L_{IR} = L(8\text{--}1000\mu\text{m})$ as measured by *Herschel*-PACS and additional information provided by the extinction corrected $H\alpha$ luminosity $L(H\alpha)$, the extinction corrected UV monochromatic luminosity $L_\nu(\text{UV})$ measured at 1528\AA rest wavelength, and SED fitting to the extinction corrected multi-band photometry of our sources.

In using L_{IR} as an SFR indicator the operational assumption is that a significant (dominant) fraction of the total bolometric stellar luminosity (L_*) of the star-forming population is absorbed and re-radiated as thermal infrared dust emission. For an unobscured population, L_* is simply the total luminosity of the directly observable stellar

³<http://galex.stsci.edu/GalexView/>

population. In converting an extinction corrected $L(H\alpha)$ to a SFR it is assumed that all of the ionizing Lyman continuum photons emitted by short-lived massive O-type stars are absorbed, photo-electrically, in the surrounding H II regions with no competition from internal dust. $L_\nu(UV)$ is a direct measure of starlight produced by mixtures of O, B, and A type stars.

For the SFR calibrations, we have used our synthesis code STARS (Sternberg 1998; Sternberg et al. 2003) to compute L_* , $L(H\alpha)$ and $L_\nu(UV)$ as functions of the “present-day” instantaneous star-formation rates ($M_\odot \text{ yr}^{-1}$), for a wide range of galaxy ages and star-formation histories. As is standard, we assume that the star-formation rates vary exponentially as,

$$SFR(t) = R_0 e^{-t/\tau} \quad (2)$$

where t is the age of the stellar population, τ is the “decay-time-scale” of the star-formation activity, and R_0 is the initial SFR at $t = 0$. In the calculations we assume Kroupa/Chabrier initial-mass-functions (IMFs) for the stellar populations. We consider ages t from 1 to 10^3 Myr, and decay time-scales τ equal to 10, 10^2 , 10^3 Myr, and also $\tau = \infty$ which corresponds to a continuous non-varying SFR.

The resulting SFR calibrations are displayed in Figure 3. The behavior may be understood by first noting that if the time-scale τ over which the SFR varies is longer than the time required for a given indicator to equilibrate, then the given indicator will linearly track the instantaneous SFR. For $L(H\alpha)$ the equilibration time is equal to the lifetime (~ 3 Myr) of the Lyc producing O-stars. Therefore, for $\tau \geq 10$ Myr $SFR/L(H\alpha)$ is a constant, independent of t or τ , as indicated by the flat line in Figure 3. For our assumed IMFs $SFR/L(H\alpha) = 2.1 \times 10^{-8} [M_\odot \text{ yr}^{-1} L_\odot^{-1}]$.

In contrast, any variation in the SFR is rapid compared to the equilibration time for L_* for which contributions from long-living low mass stars are significant. As the SFR drops rapidly the decline in L_* is moderated by the presence of the radiating longer-living stars. Therefore, for all τ SFR/L_* drops sharply when $t/\tau > 1$. Even for continuous star-formation ($\tau = \infty$) SFR/L_* declines with t , due to the continuing build-up of low mass stars.

The UV equilibration time is ~ 100 Myr, as set

by the lifetimes of A-type stars. Therefore, in Figure 3, $SFR/L(UV)$ declines with t for $t/\tau > 1$ for $\tau < 100$ Myr. However, for $\tau > 100$ Myr, the variation in the star-formation activity is sufficiently slow that the UV tracks the instantaneous SFR, and $SFR/L_\nu(UV)$ is then a constant. In this limit $SFR/L_\nu(UV) = 6 \times 10^{-7} [M_\odot \text{ yr}^{-1} L_\odot^{-1} H z^{-1}]$.

Figure 3 shows the ratios $L_\nu(UV)/L_*$ and $L_{H\alpha}/L_*$ as functions of t/τ for different combination of t and τ , in the limit ($\tau > 100$ Myr) where both $L_\nu(UV)$ and (automatically) $L(H\alpha)$ track the instantaneous SFR. The limit $t/\tau \ll 1$ is continuous star-formation, and $t/\tau \gg 1$ is “post-burst” decaying star-formation.

The following analysis is based on the comparison of various observed luminosities with the calculations presented in Figure 3. We wish to determine the values of t and τ that best match the observed L_* , $L_\nu(UV)$, and $L(H\alpha)$. If only the L_{IR} is considered, and viewed as a measure of L_* for young ($t/\tau \ll 1$), dusty star-forming regions, then for our assumed IMF $SFR(IR) \simeq 1.1 \times 10^{-10} L_{IR}/L_\odot$.

The post-starburst scenario implies that these objects had a higher SFR in the past, e.g., assuming the exponentially decaying star formation histories and parameters as listed in Table 3, they were typically forming stars more actively by a factor 25 at $z=1$, implying star formation rates of about $60 M_\odot \text{ yr}^{-1}$ at that time. Their SFR were up to 10 times faster than those estimated in normal star forming galaxies with a SFR- z relation of the kind $(1+z)^q$.

3.2. L_{FIR} measurements

The PACS FIR observations provide good estimates of L_{IR} and hence of the total stellar luminosities L_* produced in the dusty star-forming regions. The PACS measurements thus provide robust estimates of the SFRs in the optically obscured regions, which may dominate the total star-formation activity of the host galaxies. The IR applies to the entire galaxy and is not affected much by the source geometries or the central AGNs. For galaxies with detections in both PACS bands we use an SED fitting algorithm similar to Chary-Elbaz (CE)⁴. A collection of fits is shown in Fig-

⁴http://david.elbaz3.free.fr/astro_codes/chary_elbaz.html

ure 4. We also show the 24 and 70 μ m *Spitzer*-based luminosities when available, but these measurements were not included in the fits because of the very different resolutions of the two instruments. However, *Spitzer* luminosities are consistent with the best selected SED in most cases, confirming the reliability of the fits. This also suggests that AGN contribution to the 24/(1+z) μ m luminosity is small. Thus the MIR luminosity in most of our PACS-detected LINERs is not dominated by a central AGN “obscuring torus”.

For galaxies detected in one band only, we experimented with relationships of the type $L_{IR} = a + b \log L(\lambda)$ where λ refers to the detection band. Such approximations have been used successfully in several earlier studies, e.g. Symeonidis et al. (2008). Given the nature of our sources, for single-band detections we prefer to estimate L_{FIR} assuming the $L(160\mu\text{m})/L(100\mu\text{m})$ ratio is comparable to the mean ratio of 1.975 in our sample. The calculated mean does not include the three brightest objects in our sample, 825904, 827818 and 833627, with ULIRG-type luminosities of approximately $10^{12}L_{\odot}$.

Our infrared SED fits can also be used to derive a single dust temperature for the SF regions. We estimated this temperature in two ways assuming grey body emitters with an emissivity index $\gamma = 1.5$ (see Gordon et al. 2010, for discussion and a justification of the method). First, we solve for the temperatures that gives peaks in λL_{λ} that matches the maxima in our fitted SEDs. Second, we find the dust temperatures that best fit the measured $L(160/(1+z))/L(100/(1+z))$ ratios. As demonstrated in Hwang et al. (2010), the two methods give very similar results.

Figure 5 shows a plot of $T(\text{dust})$ vs L_{IR} for the 18 sources with two PACS detections. The diagram may suggest a weak tendency for more luminous sources to have hotter dust, but this correlation does not appear statistically significant. The three ULIRGs in the sample have the highest dust temperature which is consistent with the well known trend found in other samples. A more interesting result perhaps is the tendency of many sources to show low dust temperatures which puts basically all our LINERs, except for the three ULIRGs, below the median temperature line of Hwang et al. (2010).

3.3. $L_{\nu}(UV)$ measurements

As explained, we used the observed FUV and NUV fluxes to calculate the spectral slope β and the (rest) 1528 \AA luminosity $L_{\nu}(UV)$. This has been done for sources with $z < 0.41$. The limit on the redshift is due to the short wavelength side of the FUV band that, otherwise, includes part of the dropping stellar continuum below about 950 \AA rest wavelength, the Lyman break and the Ly α absorption line. Another uncertainty in the value of β is the possible contribution of the Ly α emission line to the FUV flux. We also compared the β -based extinction estimates with the E(B-V) estimates obtained from the global (i.e. entire galaxy) SED fits (see § 3.5 below). The SED fit procedure allows reddening by galactic type extinction of up to E(B-V)=0.5 mag. The values obtained in this way are considerably smaller than the value derived with the β method.

IRX, the ratio between the IR and the FUV fluxes, is a measure of extinction because it relates the dust-absorbed UV flux to the reprocessed IR flux. Meurer et al. (1999) found an empirical relationship between β and IRX in galaxies at $z \sim 3$ and Seibert et al. (2005) applied the same relation to a sample of local galaxies. Such an approximation is appropriate assuming the IR and the extincted FUV arise from the same regions. We do not find a similar relationship in our LINER sample. The reasons may be uncertainties in deriving β , the presence of a nuclear AGN source in some of the objects, or in wrong FUV modelling.

3.4. $L(H\alpha)$ measurements and reddening estimates

In analyzing the $H\alpha$ observations we considered two alternatives: most of the Balmer line emission is produced in star-forming H II regions or in AGN photoionized gas.

For star-formation, we estimate the intrinsic $H\alpha$ flux for the entire galaxy assuming that H II regions outside of the 1 “zCOSMOS slit contribute in proportion to the surface area of the galaxy covered by the aperture. We used an estimate based on the measured i_{AB} mag. inside the slit and for the entire galaxy (zCOSMOS project, private communication). Visual inspection suggests that the B and i -band images have similar dimensions confirming that the i -band magnitudes

provide reasonable measures of the relative fluxes emitted by early type stars inside and outside the slit.

We apply a standard galactic (screen) extinction correction using the observed Balmer-decrement $H\alpha/H\beta$ to estimate the intrinsic $H\alpha$ flux within the spectroscopic aperture. We assume that the derived extinction correction factors also apply to the extrapolated estimates for the $H\alpha$ emission outside the slit. The extinction corrections are uncertain because of the relatively low S/N, the weakness of the $H\beta$ line, and the severe blending of $H\beta$ with stellar features next to the line. For many objects the measured $H\alpha/H\beta$ ratios are below the case-B value of 2.8. For these objects we assume zero extinction.

We have also experimented with the correction suggested by Calzetti et al. (2007) for young (continuous) star-forming regions,

$$L(H\alpha)_{corr} = L(H\alpha_{obs}) + (0.031 \pm 0.006)L(24\mu m). \quad (3)$$

where $L(24\mu m)$ is the $24\mu m$ (dust) luminosity. The value of $L(H\alpha)_{corr}$ obtained from eqn. 3 is larger by a factor ~ 10 compared to the one obtained from the observations using the $H\alpha/H\beta$ -based reddening. This may indicate that a screen model is not appropriate for the star-forming regions (Bell 2003; Koyama et al. 2010; Villar et al. 2008, 2011) or a basic flaw in estimating $L(H\alpha)$ from the narrow slit observations.

We did not intend to study deeply SFR estimation based on $H\alpha$ and UV measurements, because we have not good enough data, as we said above.

3.5. Optical-MIR SED fitting and stellar mass determination

All 97 LINERs in our sample also have broad band photometric observations ranging from the U-band to the $24\mu m$ mid-IR. These data are presented in Bongiorno et al. (2010), who fit the optical to mid-IR spectral SEDs, yielding photometric estimates of the galaxy stellar masses. In these fits, the resulting system ages are large, $\gtrsim 10^9$ yr, and significantly greater than the inferred star-formation decay times. Furthermore, extinction corrections are small. Thus, the optical-MIR SEDs are probing the predominantly unobscured and evolved stellar populations that comprise the bulk stellar mass of the LINER host

galaxies. The stellar masses has been computed using the 2-components SED fitting technique described in Bongiorno et al. in preparation and are listed in Table 2. We note that the stellar bolometric luminosities L_* inferred from the optical-MIR SED fitting are comparable (within a factor ~ 2) to the IR luminosities inferred from the PACS observations.

The instantaneous SFRs derived from the optical-MIR SED fitting for the evolved populations are $\sim 1 M_\odot \text{ yr}^{-1}$, significantly smaller than the $\sim 10 M_\odot \text{ yr}^{-1}$ inferred from the FIR assuming that the FIR is tracing continuous star-formation in young star-forming regions.

To summarize, there are two distinct possibilities. (a) the FIR traces young (steady) star-forming regions for which

$\text{SFR}/L_{IR} \simeq 10^{-10} [M_\odot \text{ yr}^{-1} L_\odot^{-1}]$ depending only on the assumed IMF. A possible reason for the very different results obtained from the SED fitting is the large obscuration of the H regions where more of the SF activity is taking place. Such regions contribute little, if anything to the bands used in the SED fitting process. (b) the FIR is reradiated luminosity from the evolved post-burst population for which SFR/L_{IR} is declining and depends on the system age t and decay time-scale τ , as inferred from the SED fitting and $H\alpha$ and UV luminosities. The difficulty here is the large amount of dust, and its distribution through the galaxy, necessary to explain the high L_{FIR} . The inferred SFRs for both options are listed in Table 3 together with the values of t and τ for the postburst decay model. The value of M_* obtained from the SED fit is basically independent of the two assumptions and hence we use it in the following analysis.

We have used the above estimates of SFR and M_* to construct two SFR vs. M_* diagrams (Figure 6). For reasons discussed below, we consider the SED derived M_* to represent well the two possibilities. Both diagrams show SFRs based on the measured L_{FIR} which is the one least affected by the observational uncertainties. The diagram includes 34 LINERs with at least one *Herschel* detection and two stacks representing the remaining 40 sources with *Herschel* upper limits, see § 2.2. The uncertainties on the masses are obtained from the SED fitting procedure and reflect only the photometric uncertainties. Uncertainties on SFRs are

only observational and reflect the uncertainty on the PACS photometry. They do not include the uncertainty in FIR SED fitting. The uncertainties on the stacked data are due to the scatter between sources in these groups and reflect their variance (due to both intrinsic and observational errors).

SFR versus stellar mass relations in the two diagrams are very different. For model (a) (left panel) our sample lies along the “main-sequence” (MS) for star-forming galaxies. This is illustrated by the two diagonal lines that represent the mean main sequence at two redshifts, $z=0.1$ and $z=1$ from Dutton et al. (2010) and reference therein. Most of the detected LINERs lie close to the expected location of the $z=0.3$ main sequence with the three ULIRGs well above it. There is a clear tendency for the lower M_* sources (those with $M_* < 10^{9.5}$) to have smaller SFR. The consistency with the main-sequence, in combination with the HST images that show that most of the galaxies in our sample are spirals, is evidence that the FIR is in fact tracing young embedded star-forming regions, with large inferred SFRs $\sim 10 M_\odot \text{ yr}^{-1}$. Because of the large scatter from the mean values of the SFR(IR), we have calculated the average masses and SFR(IR) of the detected sources divided in 4 bins of 8 objects with similar stellar mass. We included in the mean also the stack with higher M_* considering it as a single source. According with the general result, the 3 bins including objects with higher stellar mass lie in the MS region, while the smaller mass bin lies above that region.

The right-hand panel of Figure 6 shows the positions of our galaxies assuming model (b) for which the derived SFRs correspond to postburst systems with t and τ estimated by our SED fitting procedure. The sources are well below the two MS lines as expected for passive galaxies with declining SFRs. More discussion of these findings is given in § 4.

4. Discussion

4.1. Comparison with other samples of SF galaxies

Our sample of LINER host galaxies shows clear discrepancies between various SF indicators that are based on the UV continuum, the Balmer emission lines and the FIR emission, under the assumption of continuous starburst. Such discrepancies

have been found in previous studies. For example, Rigopoulou et al. (2000) estimated $\text{SFR}(H\alpha_{obs})$ up to an order of magnitude smaller than $\text{SFR}(\text{IR})$ in their $15\mu\text{m}$ selected sample of starburst galaxies at $z>0.4$. The typical $\text{SFR}(\text{IR})$ in their sample is somewhat larger than the one we find in the LINER sample using the *Herschel*-based estimates. However, their $\text{SFR}(H\alpha_{obs})$ is about ten times larger than ours. Cardiel et al. (2003) found $\text{SFR}(H\alpha)>\text{SFR}(\text{UV})$ in a sample ($z\sim 0.4$ and 0.8) with a mean $\text{SFR}(H\alpha)$ larger than ours by about a factor 6. They also found that $\text{SFR}(H\alpha)$ consistently underestimate the SFR and the discrepancy is larger for higher L_{IR} for a continuous burst. In a sample of $15\mu\text{m}$ selected LIRGs at $0.1 < z < 0.8$, Flores et al. (2004) obtained $\text{SFR}(\text{IR})$ comparable to ours for low- z galaxies. However, their $\text{SFR}(H\alpha)$ is considerably larger than ours and agrees better with the one based on L_{IR} . These authors suggested emission from two different regions in the galaxy with different amount of obscuration, similar to our case a (§3). Finally, Liang et al. (2004) obtained the same results of Flores et al. (2004) in their $15\mu\text{m}$ selected galaxy sample at $z < 1$.

A general discussion of the various methods and the merit of extinction correction methods is given in Wuyts et al. (2011). These authors used *Herschel*-PACS data and compared them with various other observations mostly at high redshifts. They discussed the way UV, $H\alpha$ and FIR-based estimates can be reconciled by using proper dust attenuation correction factors. They find clear evidence for deviation of the various method at $\text{SFR}>100M_\odot\text{yr}^{-1}$ but the sample is not complete enough at low redshift and low SFR to compare with the present LINER sample.

The main conclusion of the above comparison is that SFR estimates based on $L(H\alpha)$ are problematic and tend to be underestimated even in sources (LIRGs or high SFR high- z galaxies) where the assumption of a continuous burst is justified and it is not possible to apply to a decaying scenario.

4.2. Color morphology and SF in LINER host galaxies at $z=0.3$

We adopt the morphology based on HST images as listed in the IPAC Archive⁵. This reference classifies 24 sources as spirals, 7 as ellipticals, and 3 as irregular galaxies (see Table 1). Additional inspection of the HST images suggests that some, perhaps even all sources classified as elliptical galaxies may in fact be disk systems. This supports the idea that most of our sources contain H regions that are likely to be outside the 1" slit (assuming it was placed across the centers of these galaxies).

We have also looked at the color of the sources as derived from the multi-band photometry. Most objects have reddish colors and are similar in this respect to the much larger COSMOS galaxy sample discussed in detail in Bongiorno et al. (2010). This again is consistent with a combination of old stellar population and highly obscured H regions in the disk. The alternative is that the red color is due to reddening and extinction. Unfortunately, our broad band photometry which lacks information on the very short wavelengths is insensitive to such reddening.

4.3. SFRs and AGN luminosity in local and $z=0.3$ LINERs

We now consider the possibility that most of the line emission inside the 1" slit is from AGN-ionized gas. We can then compare the AGN and the SF luminosities to those observed in local LINERs. Our estimated bolometric AGN luminosities, $L(\text{AGN})$, are based on the approximation given in Netzer (2009),

$$\log L(\text{AGN}) = \log L(H\beta) + 3.75 + \max[0.0, 0.31 \times (\log \frac{[OIII]}{H\beta} - 0.6)], \quad (4)$$

where $L(H\beta)$ is the galactic extinction corrected $H\beta$ luminosity. A more accurate estimate of $L(\text{AGN})$ in LINERs is based on a combination of $L([OIII]\lambda 5007)$ and $L([OI]\lambda 6300)$ (Netzer (2009)). This cannot be used in the present case since the weaker $[OI]\lambda 6300$ line is not observed in most of the $z=0.3$ LINERs. We do not correct the Balmer line flux for the aperture size because we

consider only nuclear emission line regions (this assumption was also used in Bongiorno et al. 2010). Given this approximation, we find that the AGN bolometric luminosity in our sample is between $10^{42.6}$ and $10^{44.9}$ erg/sec.

Considering that all the L_{IR} is due to SF, thus $L_{SF}=L_{IR}$, we compared $L(\text{AGN})$ and L_{IR} in our LINER sample with those of the local ($z \leq 0.01$) LINERs studied by Ho et al. (1997) using only objects classified as type-II LINERs. For most of the local LINERs we can use the IRAS 60 μ m and 100 μ m fluxes and the expression provided in Sanders & Mirabel (1996),

$$F_{FIR} = 1.26 \times 10^{-14} (2.58 \times F(60\mu m) + F(100\mu m)) \text{ Wm}^{-2}, \quad (5)$$

where $F(60\mu m)$ and $F(100\mu m)$ are the fluxes in the relevant IRAS bands, to obtain L_{SF} . We do not include the IRAS 12 and 25 μ m fluxes since they may be influenced by warm AGN-heated dust. We also calculated $L(\text{AGN})$ for all these sources using the same method as for the *Herschel* detected LINERs. The resulting L_{IR} vs. $L(\text{AGN})$ for the two samples is shown in Figure 7. The diagram shows also a line indicating the location of AGN dominated objects from Netzer (2009). Local LINERs show considerably lower $L(\text{AGN})$ and L_{SF} and the two samples form a continuous sequence in both properties.

There are several possible reasons for the very different properties of the two groups. First, in local LINERs the line emission is from the very nuclear region of the galaxy which is much smaller, in terms of physical size, than the regions covered by the 1" slit in the $z \sim 0.3$ sample. Second, while most of the $z=0.3$ LINERs have not been detected by *Herschel*, our comparison is based on objects that were selected to have the largest L_{SF} . The undetected sources (stacked data) have lower L_{SF} closer to what has been observed in the local LINERs. Third, there may well be a population of local ($z < 0.1$) LINERs with higher L_{SF} that have not been studied, systematically, with sensitive FIR instruments. Finally, there may be a real evolution in the AGN and SF properties of LINER host galaxies between $z=0$ and $z \sim 0.3$, but to test this idea there is no systematic study based on FIR observations of LINERs at a large range of redshift.

The gap between the 2 samples may also be

⁵IPAC Infrared Science Archive (IRSA) - Cassata Morphology Catalog v1.1

due to a selection effect, because the fainter FIR sources are not included in the diagram. To test this we plotted on this diagram $L(\text{AGN})$ vs $L(\text{IR})$ for the two stacks shown in Figure 6. If $M_* > 10^{9.5}$, the stacked source lies in the $z \sim 0.3$ LINERs region. For smaller M_* the stacked source descends into the gap region, but its IR measurement is only an upper limit, which may effect the correlation.

4.4. Revised diagnostic diagrams for LINERs

Our new FIR observations, and stellar evolution analysis, suggest that LINER like spectra from the inner parts of early type galaxies are not necessarily related to old stellar populations. Obscuration in the nucleus and the disk can hide much of the line emitting gas (Sturm et al. 2006; Dudik et al. 2009) and post-starburst behaviour, as discussed here, (§ 4.2) can result in large L_{FIR} . This raises several general questions regarding the usefulness of some of the commonly used line diagnostics in galaxies showing high L_{IR} and obscuration.

Spectroscopic studies of LINERs in the local universe, e.g. SDSS LINERs, indicate low extinction as judged from the observed $H\alpha/H\beta$ line ratio (e.g. Kauffmann et al. 2003). These observations refer to the inner 3" part of the host galaxy (the diameter of the SDSS fiber used for spectroscopy). In contrast, highly ionized type-II sources show a clear correlation of extinction with SFR as measured by the $D_n4000\text{\AA}$ index and by *Galex* UV observations (e.g. Salim et al. 2007, and references therein). The mean $H\alpha/H\beta$ in our $z \simeq 0.3$ sample is also small (about 50% of the *Herschel*-detected LINERs have $H\alpha/H\beta < 2.8$, i.e. consistent with no reddening) yet L_{IR} is high which suggest high obscuration in H regions mostly outside the 1" slit. Thus, the spectroscopic definition of LINERs, which is based on the observed $[OIII]/H\beta$ and $[NII]/H\alpha$ line ratios, can critically depend on the aperture size and the H regions distribution, and extinction, in the disk. We suspect that larger aperture spectroscopic observations of our LINERs will reveal composite LINER/ H II spectra.

The general issue of composite vs. "pure" AGN spectra has been discussed in various papers, most recently by Wild et al. (2010). This paper as-

sesses the fraction of high ionization AGNs in three groups, SF galaxies, composite SF-AGN objects and pure AGNs. We suggest that our LINER classified objects would be considered composite SF-LINER objects had they been observed with larger spectroscopic aperture. A complex geometry can contrive to mix LINERs and H II regions and confuse the standard spectroscopic diagnostics.

Another possibility that was already mentioned is related to extreme obscuration in compact, luminous H II regions. The obscuration in such H II regions can be so large that the standard use of the $H\alpha/H\beta$ line ratio to correct for extinction may not be valid. One must therefore consider the possibility that "pure" LINERs, with emission lines that are excited exclusively in AGN photoionized gas, cannot be unambiguously identified in galaxies with large SFRs. The temperatures that we estimated for those galaxies with two PACS detections seem to be not high enough to be related to compact H regions, but their measurements suffer from uncertainty due to observations and modelling, so that we cannot exclude the existence of those heavy obscuring H regions.

5. Conclusions

We present the first systematic study of the FIR properties of LINERs at $z \sim 0.3$. The sample includes 96 LINERs from the first release of zCOSMOS and their emission line properties have been studied by Bongiorno et al. (2010). The main findings of the work are:

1. 34 of the sources have $\sigma > 3$ detections in at least one *Herschel*/PACS band. The mean L_{FIR} in this group is about $10^{44.5}$. We were able to divide the remaining sources in two groups according to their M_* . Stacking sources in the first ($M_* > 10^{9.5}$) group gave a significant mean $L(\text{IR})$ signal. The remaining sources with $M_* < 10^{9.5}$ provided only upper limit.
2. Assuming that the FIR arises in young star-forming regions, the FIR luminosities imply typical star-formation rates of $\sim 10 M_\odot \text{ yr}^{-1}$.
3. Almost all LINERs have FUV and/or NUV *Galex* detections. The UV flux is slightly larger for objects with PACS detections.

However, the SFRs obtained with the UV-corrected fluxes are low compared to the SFRs inferred from the *Herschel* measurements, assuming the UV is produced in young star-forming regions producing the FIR.

4. The assumption that *all* the $H\alpha$ line flux is due to SF was used to obtain $L(H\alpha)$ -based SFRs. These are also considerably smaller than the FIR-based SFRs assuming young-and-steady star formation. The reason of this gap may be the inaccuracy of the $H\alpha$ and UV extinction estimates. Alternatively, the $H\alpha$ and UV may be tracing residual “post-burst” star-formation in the older underlying population and they may not be associated with the ongoing star-forming regions that produce the FIR.
5. The assumption that *all* the $H\alpha$ line flux is due to SF was used to study two, different SF scenarios. The first assumes continuous SF in highly obscured HII regions and the second a post-starburst decay. Both scenarios have their own short-comings but the first seems to agree better with the observations including the fact that the HST images of most sources show evidence for disk-type systems. Under the more favorable assumption, almost all of the *Herschel* detected LINERs are situated on the MS in the SFR vs. M_* diagram.
6. All our *Herschel* detected LINERs are situated above the location of local LINERs in the L_{SF} vs. $L(\text{AGN})$ diagram.
7. The present work raises the possibility that simple optical line diagnostic diagrams based on spectroscopy of the central parts of galaxies can indicate a typical LINER spectrum in cases where the host galaxy undergoes enhanced SF activity.

We acknowledge Roberto Maiolino and David Rosario for the useful comments and the DFG for support via German-Israeli Project Cooperation grant STE1869/1-1/GE625/15-1.

TABLE 1
SAMPLE

ID	z	R.A. (deg)	Dec (deg)	<i>Herschel</i> PACS 100 μ m	<i>Herschel</i> PACS 160 μ m	<i>Spitzer</i> IRAC, MIPS	FUV (μ Jy)	eFUV (μ Jy)	NUV (μ Jy)	eNUV (μ Jy)	β	Morphology *
804277	0.361	150.41975	1.7757300	X	X	X	1.45	0.10	3.83	0.12	-0.41	1
805283	0.266	150.19297	1.7524000	X	X	X	3.12	0.11	7.34	0.15	-0.12	2
810944**	0.347	150.34825	1.9489800	X	X	X	0.24	0.08	1.12	0.21	-1.79	2
812596	0.342	149.98805	1.8229900	X	X	-	2.41	0.11	5.62	0.15	-0.10	2
816998**	0.425	150.41833	2.0851500	X	X	X	0.77	0.14	1.78	0.14	-0.07	2
818160	0.347	150.18249	2.0393300	X	X	-	1.22	0.32	1.75	0.42	1.10	2
818453	0.360	150.12748	2.1122300	X	X	-	-	-	-	-	-	2
819347	0.356	149.92088	2.0312300	X	X	X	-	-	2.93	0.51	-	2
820454	0.354	149.63649	2.0201200	X	X	-	1.18	0.12	3.90	0.20	-0.96	2
825006	0.345	150.06764	2.2429900	X	X	X	0.89	0.10	3.69	0.13	-1.52	2
825904	0.344	149.89498	2.2084100	X	X	X	2.74	0.36	7.04	0.59	-0.34	3
827762	0.282	149.50944	2.2318800	X	X	X	4.47	1.55	6.12	1.46	1.22	2
827818	0.305	149.49485	2.2806500	X	X	X	0.52	0.09	2.14	0.11	-1.51	3
833627	0.373	149.74729	2.3457300	X	X	-	1.17	0.14	6.41	0.15	-2.21	2
839646	0.346	149.97569	2.4614300	X	X	X	-	-	2.43	0.06	-	2
845649	0.305	150.16024	2.6993000	X	X	X	1.46	0.10	3.39	0.16	-0.08	2
845945	0.350	150.10801	2.6955500	X	X	X	1.89	0.15	3.15	0.15	0.73	1
848329	0.353	149.58770	2.7614100	X	X	-	1.56	0.13	2.58	0.15	0.75	2
818456**	0.382	150.12730	2.0818700	-	X	-	-	-	-	-	-	2
827400**	0.379	149.59808	2.1583900	-	X	-	0.40	0.09	0.79	0.09	0.31	2
834427	0.445	149.59079	2.4282400	-	X	-	1.07	0.10	2.03	0.09	0.42	2
838271	0.376	150.22023	2.5245400	-	X	X	-	-	1.32	0.36	-	1
804573	0.309	150.34526	1.6993800	X	-	-	0.84	0.20	-	-	-	1
808018	0.284	149.57618	1.6434400	X	-	-	0.77	0.22	1.19	0.53	0.90	2
812330**	0.439	150.04893	1.9487800	X	-	-	-	-	-	-	-	2
818225	0.310	150.17228	2.0060500	X	-	-	0.64	0.13	1.94	0.26	-0.77	2
819241	0.356	149.94342	2.0962300	X	-	-	-	-	-	-	-	3
819596**	0.417	149.86483	2.0032800	X	-	-	0.82	0.26	-	-	-	2
823616	0.255	150.36183	2.2647600	X	-	-	4.40	0.12	7.83	0.16	0.58	2
830317	0.374	150.38441	2.3912700	X	-	-	0.43	0.14	2.01	0.22	-1.83	2
832130	0.371	150.03523	2.4151200	X	-	-	-	-	0.72	0.23	-	1
832902	0.333	149.88401	2.4583800	X	-	-	4.25	1.74	14.69	2.67	-1.08	2
833279**	0.426	149.81184	2.4412200	X	-	-	-	-	-	-	-	2
842079	0.419	149.47718	2.5823700	X	-	-	0.61	0.07	0.89	0.09	1.07	1

*IPAC Infrared Science Archive (IRSA) - Cassata Morphology Catalog v1.1: 1. spiral; 2. elliptical; 3. irregular

**Optical lines S/N<3

TABLE 2
LUMINOSITIES

ID	L_{IR} L_{\odot}	L_{IR}^* L_{\odot}	$L(H\beta)$ L_{\odot}	$L(AGN)^{**}$ L_{\odot}	M_*
804277	11.24	11.22	6.87	10.62	10.967
805283	10.96	10.96	6.93	10.68	10.977
810944	10.96	10.69	8.95	12.70	11.18
812596	10.73	-	8.11	11.85	10.781
816998	11.27	11.56	7.55	11.30	10.29
818160	10.86	-	5.89	9.64	10.67
818453	11.14	-	5.76	9.51	9.11
819347	11.05	10.71	7.21	10.96	11.033
820454	11.08	-	6.58	10.33	11.028
825006	11.18	10.97	7.21	10.96	10.891
825904	11.99	11.94	6.92	10.67	10.368
827762	11.10	11.00	7.84	11.59	10.941
827818	11.88	11.78	7.49	11.24	10.7
833627	11.97	-	7.45	11.20	11.441
839646	11.04	11.12	6.78	10.53	10.915
845649	10.83	11.03	6.99	10.74	10.736
845945	11.43	11.51	7.67	11.42	10.804
848329	11.13	-	6.94	10.69	11.077
818456	10.83	-	6.32	10.07	9.46
827400	10.74	-	7.33	11.08	10.2
834427	11.02	-	6.81	10.56	9.723
838271	11.09	11.01	6.97	10.72	10.39
804573	10.45	-	6.90	10.65	10.895
808018	10.31	-	6.77	10.52	10.967
812330	10.91	-	7.42	11.17	9.93
818225	10.42	-	6.31	10.06	10.722
819241	10.86	-	6.15	9.90	9.27
819596	10.96	-	6.27	10.02	9.19
823616	10.39	-	6.72	10.47	10.077
830317	10.87	-	6.78	10.53	10.787
832130	10.55	-	6.39	10.14	10.144
832902	10.93	-	7.13	10.88	10.074
833279	11.00	-	6.49	10.24	10.02
842079	10.81	-	6.99	10.74	10.108

* L_{IR} estimated by Kartaltepe et al. (2010).

** (AGN) estimated as in Netzer (2009).

TABLE 3
STAR FORMATION RATES

ID	SFR(IR) ¹ M _⊙ yr ⁻¹	t ² 10 ³ Myr	τ ² 10 ³ Myr	SFR(IR) τ = ∞ M _⊙ yr ⁻¹	SFR(Hα) ³ M _⊙ yr ⁻¹	SFR(Hα) ⁴ M _⊙ yr ⁻¹
804277	2.68	7.00	2.00	17.38	1.46	0.36
805283	2.75	7.00	2.00	9.12	0.47	0.17
810944	-	-	-	9.12	222.29	52.80
812596	1.99	9.00	3.00	5.37	14.95	7.59
816998	-	-	-	18.62	3.06	1.47
818160	0.50	9.00	2.00	7.24	0.12	0.04
818453	0.13	2.00	0.60	13.80	0.06	0.03
819347	1.34	5.00	1.00	11.22	2.59	0.97
820454	1.33	5.00	1.00	12.02	0.57	0.20
825006	2.56	9.00	3.00	15.14	1.49	0.65
825904	-	-	-	97.72	0.73	0.37
827762	2.52	7.00	2.00	12.59	11.98	4.09
827818	0.003	3.00	0.60	75.86	3.87	1.85
833627	2.94	9.00	2.00	93.33	5.06	1.68
839646	2.38	7.00	2.00	10.97	0.53	0.18
845649	1.58	7.00	2.00	6.76	1.56	0.58
845945	1.84	7.00	2.00	26.92	7.13	2.82
848329	1.49	5.00	1.00	13.49	2.22	0.52
818456	-	-	-	6.75	0.09	0.04
827400	-	-	-	5.50	2.72	1.28
834427	1.73	3.00	3.00	10.54	0.54	0.29
838271	0.71	7.00	2.00	12.40	2.16	0.56
804573	0.84	9.00	2.00	2.83	1.11	0.48
808018	0.0025	7.00	0.60	2.05	0.55	0.35
812330	-	-	-	8.14	2.31	1.58
818225	0.20	4.00	0.60	2.64	0.30	0.12
819241	9.95	0.26	30.00	7.19	0.35	0.05
819596	-	-	-	9.18	0.25	0.09
823616	1.24	2.00	0.60	2.48	1.13	0.32
830317	2.01	9.00	3.00	7.43	0.98	0.36
832130	0.47	4.00	1.00	3.57	0.31	0.13
832902	3.09	2.00	1.00	8.56	1.86	0.81
833279	-	-	-	10.01	0.25	0.17
842079	11.91	1.60	15.00	6.43	0.69	0.26

¹SFR only for LINERs with line S/N>3;

²t, τ are obtained as in § 3.1;

³Hα corrected for extinction and aperture;

⁴Hα corrected only for extinction.

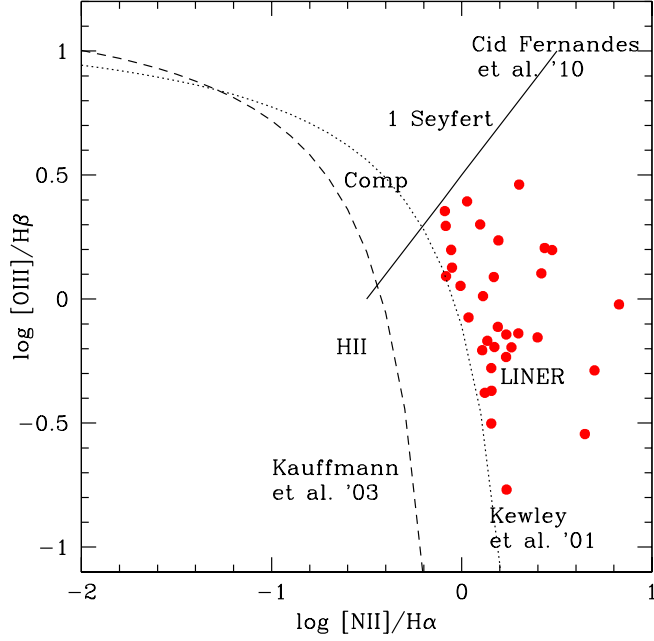


Fig. 1.— BPT diagram of the LINERs in our sample: The dotted line marks the separation between AGN and starburst galaxies (Kewley et al. 2001) The dashed line defines the region with composite objects (Kauffmann et al. 2003) and the solid line divides LINERs from Seyfert 2 galaxies (Cid Fernandes et al. 2010).

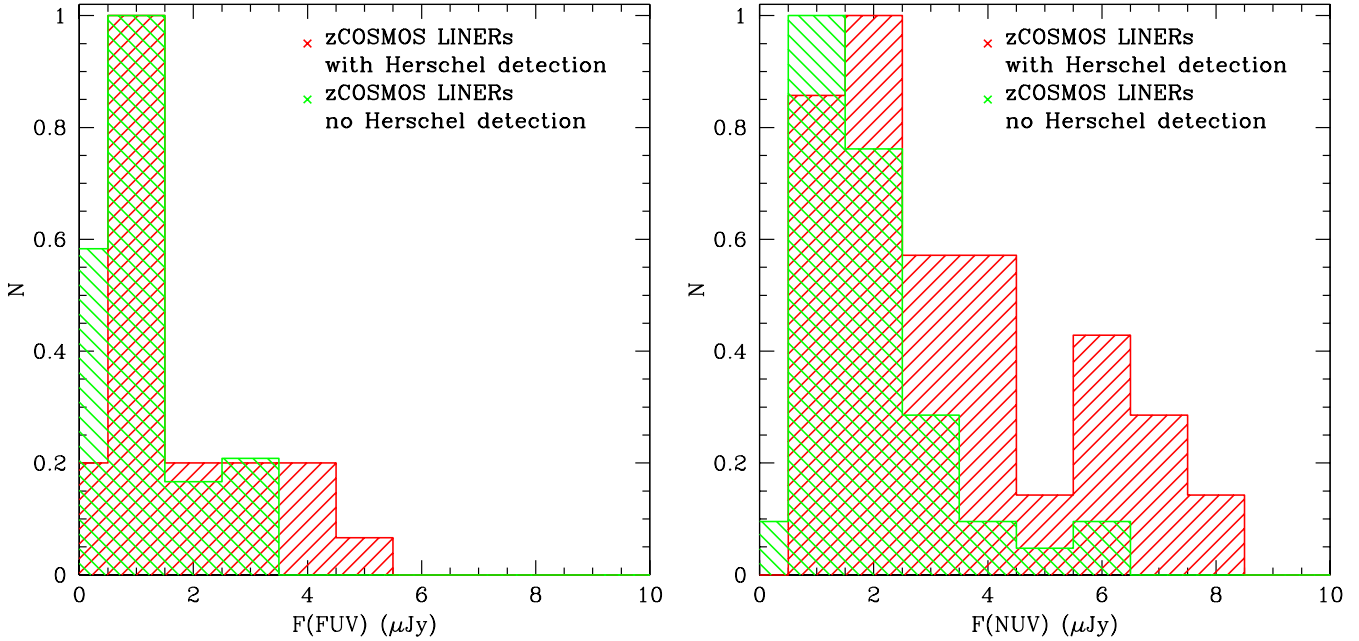


Fig. 2.— FUV (left panel) and NUV (right panel) flux distributions for detected and undetected LINERs.

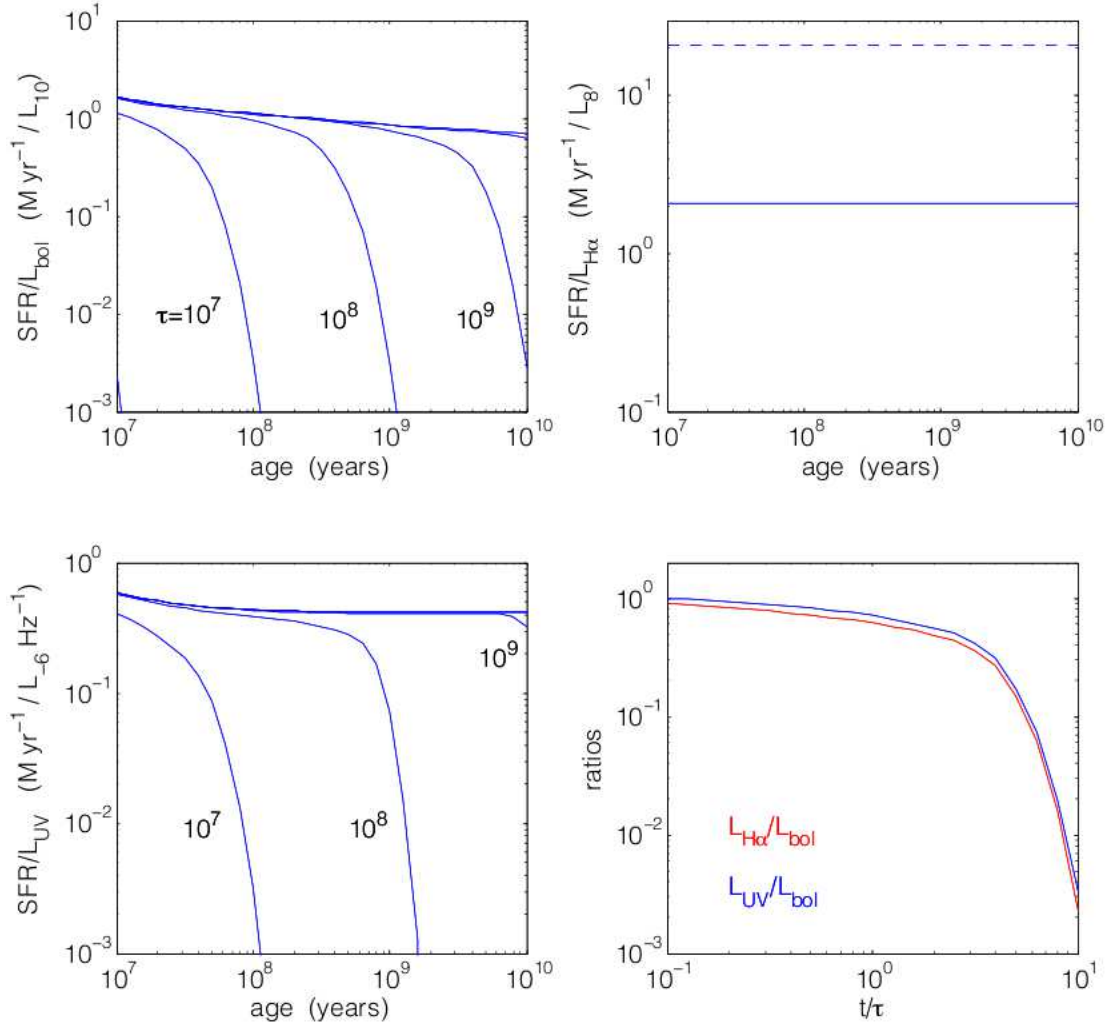


Fig. 3.— SFR calibrations for L_* , $L(H\alpha)$, $L_\nu(\text{UV})$ for $t=10\text{--}10^4\text{Myr}$ and $\tau=10\text{--}10^3\text{Myr}$. $\tau = \infty$ corresponds to continuous SFR.

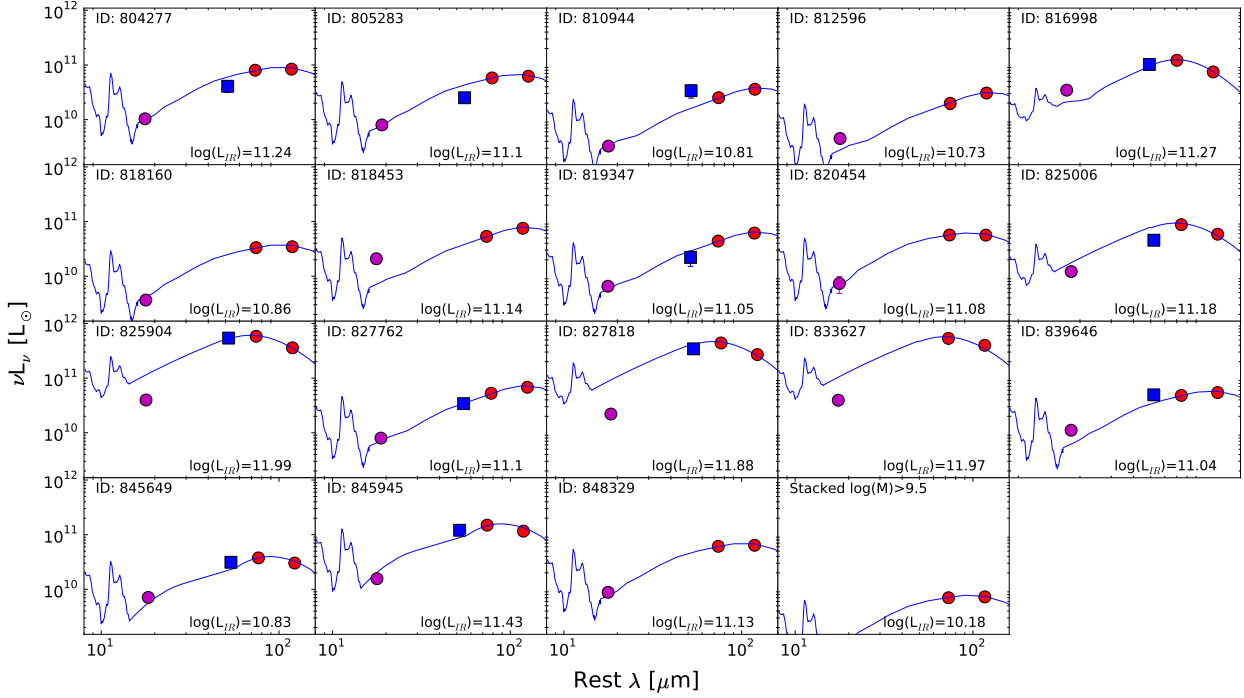


Fig. 4.— SED fittings of *Herschel* detected LINERs in both the 100 μ m and 160 μ m PACS bands. Also shown are the available 70 μ m and 24 μ m *Spitzer* observations. The SED fits use only the PACS observations.

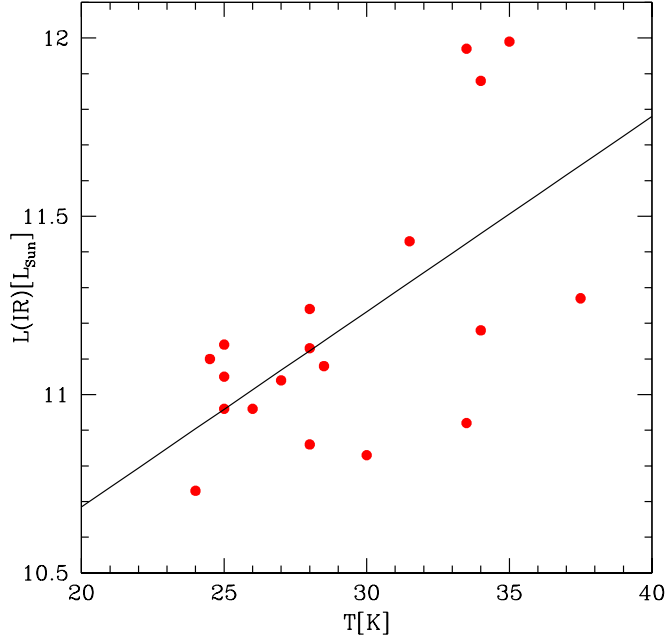


Fig. 5.— Single Grey-body temperatures with $\gamma=1.5$ vs. L_{IR} for 19 LINERs with 100 μ m and 160 μ m PACS observations. The solid line fits the data.

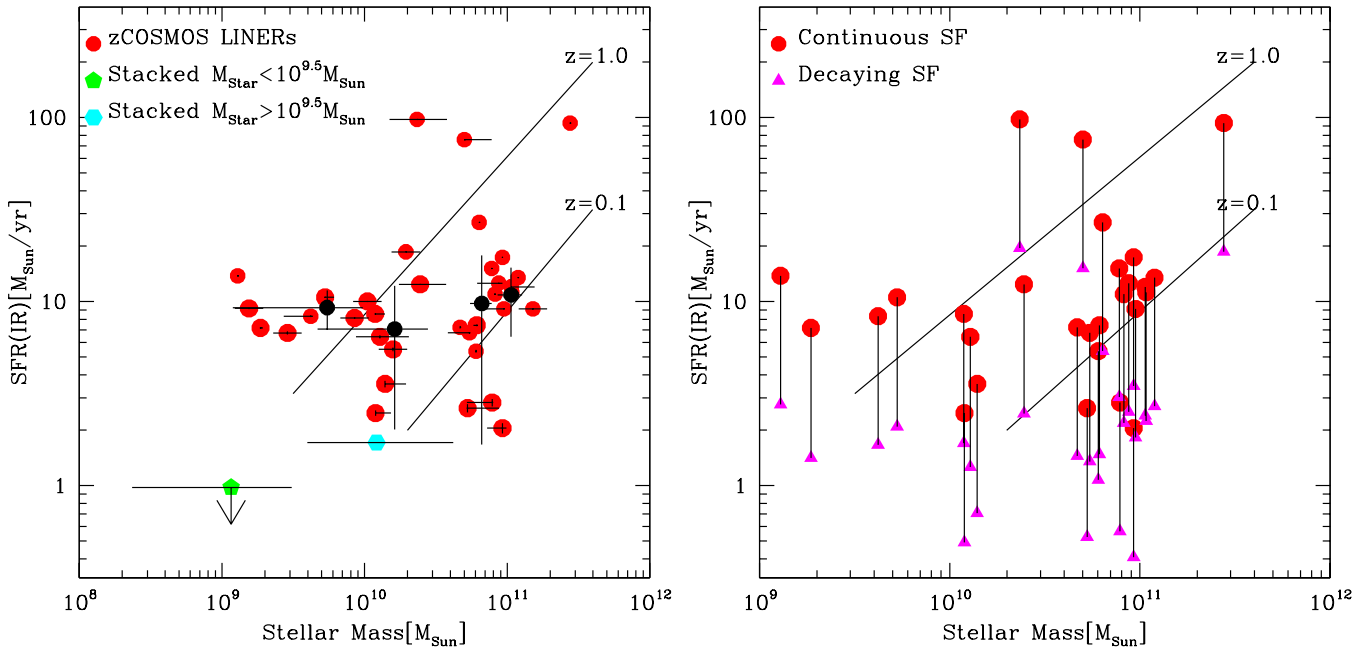


Fig. 6.— **Left panel:** SFR vs. stellar mass for the LINER sample. Plotted are 34 objects detected by *Herschel* with $\sigma > 3$, red circles, and stacked point, the green pentagon and the cyan hexagon. Black circles show the average of SFRs in mass bins of 8 objects. The error bars represent the standard deviation in the bin. **Right panel:** SFR vs. stellar mass for *Herschel* detected objects considering two possibilities: as continuous SF galaxies (red circles) and post-starburst systems with t and τ as in § 3.1 (magenta triangles).

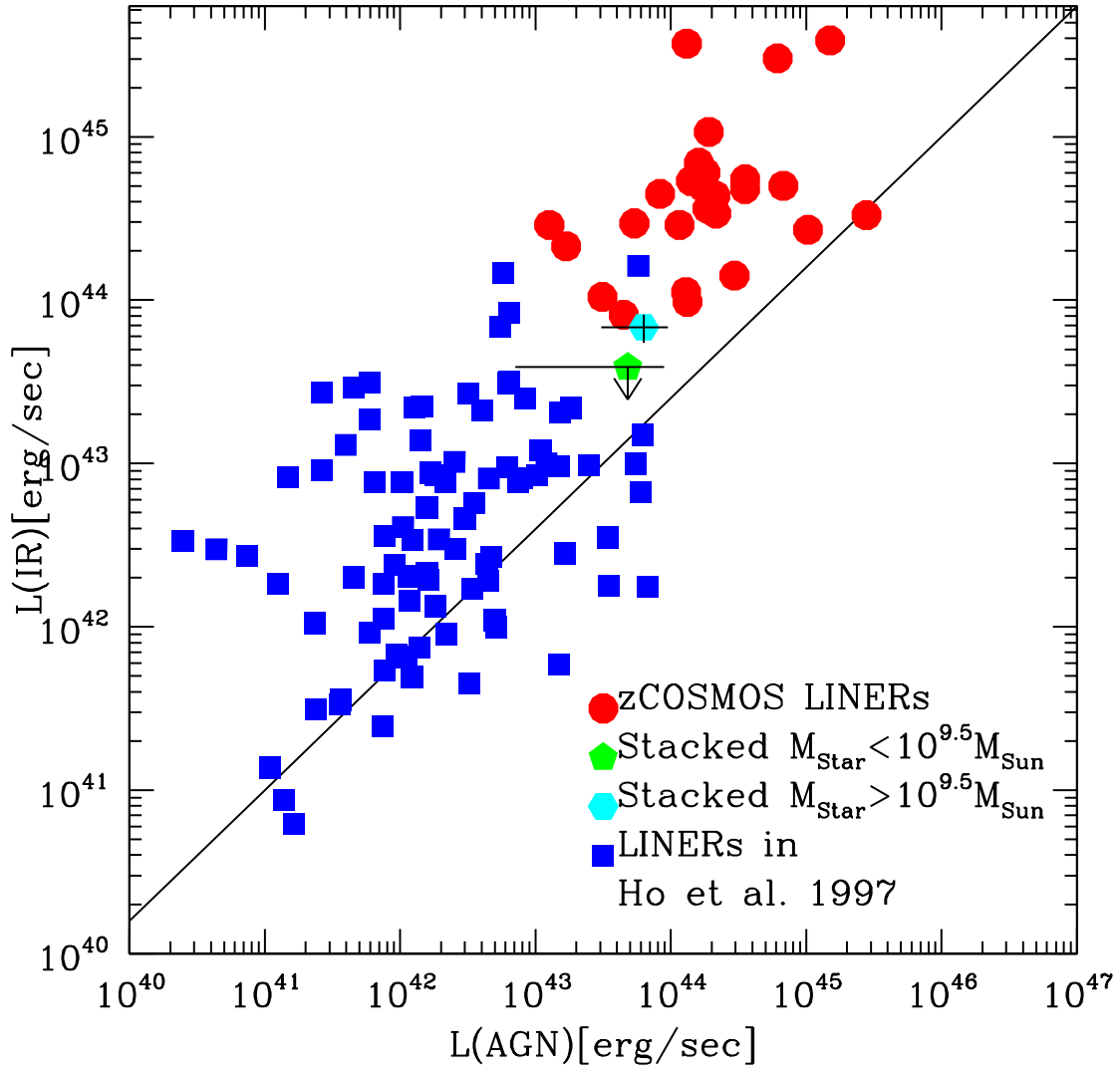


Fig. 7.— $L(\text{AGN})$ as in Netzer (2009) versus L_{IR} in our sample and in Ho et al. (1997). The $L(\text{AGN})$ of the stacked sources is the average $L(\text{AGN})$ of the binned sources and the error bars are the standard deviation from the mean. The solid line is the empirical relationship for AGN-dominated sources from Netzer (2009).

REFERENCES

- Annibali, F., Bressan A., Rampazzo R., Zeilinger W. W., Vega O., Panuzzo P. 2010, A&A 519, A40
- Baldwin, J. A., Phillips, M. M., Terlevich, R. 1981, PASP, 93, 5
- Barth, A. J., Ho, L. C., Filippenko, Alexei V., Sargent, W. L. W. 1998, ApJ, 496, 133
- Bell, E. F. 2003, ApJ, 586, 794
- Berta, S. et al. 2010, A&A, 518, L30
- Bianchi, L. & The *Galex* Team 1999, MmSAI, 70, 365
- Bongiorno, A. et al. 2010, A&A, 510, A56
- Bouwens, R. J. et al. 2009, ApJ, 705, 936
- Buat, V. et al. 2007, ApJS, 173, 404
- Calzetti, D., Kinney, A. L., Storchi-Bergmann, T., 1994, ApJ, 429, 582
- Calzetti, D. et al. 2007, ApJ, 666, 870
- Cardiel, N., Elbaz, D., Schiavon, R. P., Willmer, C. N. A., Koo, D. C., Phillips, A. C., Gallego, J. 2003, ApJ, 584, 76
- Chary, R., Elbaz, D. 2001, ApJ, 556, 581
- Cid Fernandes, R., Stasiska, G., Schlickmann, M. S., Mateus, A., Vale Asari, N., Schoenell, W., Sodré, L. 2010, MNRAS, 403, 1036
- Daddi, E., Cimatti, A., Renzini, A., Fontana, A., Mignoli, M., Pozzetti, L., Tozzi, P., Zamorani, G. 2004, ApJ, 617, 746
- Dopita, M. A., Koratkar, A. P., Allen, M. G., Tsvetanov, Z. I., Ford, H. C., Bicknell, G. V., Sutherland, R. S. 1997, ApJ, 490, 202
- Dudik, R. P., Satyapal, S., Marcu, D. 2009, ApJ, 691, 1501D
- Dutton, A. A., van den Bosch, F. C., Dekel, Avishai 2010, MNRAS, 405, 1690D
- Falcke, H., Nagar, N. M., Wilson, A. S., Ulvestad, J. S. 2000, ApJ, 542, 197
- Ferland, G. & Netzer, H. 1983, ApJ, 264, 105F
- Flores, H., Hammer, F., Elbaz, D., Cesarsky, C. J., Liang, Y. C., Fadda, D., Gruel, N. 2004, A&A, 415, 885
- Gallerani, S. et al. 2010, A&A, 523, A85
- Gonzalez-Martin, O., Masegosa, J., Mrquez, I., Guerrero, M. A., Dultzin-Hacyan, D. 2006, A&A, 460, 45
- Gordon, K. D. et al. 2010, A&A, 518, L29
- Heckman, T. 1980, A&A, 87, 152
- Ho, L. C., Filippenko, A. V., Sargent, W. L. W. 1997, ApJS, 112, 315
- Ho, L. C. 1999, ApJ, 516, 672
- Ho, L. C. 2008, ARA&A, 46, 475
- Hwang, H. S. et al. 2010, MNRAS, 409, 75
- Kartaltepe, J. S. et al. 2010, ApJ, 721, 98
- Kauffmann, G. & Heckman, T. M. 2009, MNRAS, 397, 135K
- Kennicutt, R. J. 1998, ARA&A, 36, 189
- Kennicutt, R. J. et al. 2009, ApJ, 703, 1672
- Kewley, L. J., Heisler, C. A., Dopita M. A. 2001, ApJS, 132, 37
- Kewley, L. J., Groves, B., Kauffmann, G., Heckman, T. 2006, MNRAS, 372, 961
- Kauffmann, G. et al. 2003, MNRAS, 346, 1055
- Koyama, Y., Kodama, T., Shimasaku, K., Hayashi, M., Okamura, S., Tanaka, I., Tokoku, C. 2010, MNRAS, 403, 1611K
- Kroupa, P. 2001, MNRAS, 322, .231K
- Laird, E. S., Nandra, K., Adelberger, K. L., Steidel, C. C., Reddy, N. A. 2005, MNRAS, 359, 47
- Leitherer, C., Heckmann, T. 1995, ApJS, 96, 38
- Liang, Y. C., Hammer, F., Flores, H., Elbaz, D., Marcillac, D., Cesarsky, C. J. 2004, A&A, 423, 867
- Lilly, S. J. et al. 2007, ApJS, 172, 70

- Lutz, D., Veilleux, S., Genzel, R. 1999, ApJ, 517, L13
- Lutz, D. et al. 2011, A&A, 532A, 90L
- Maoz, D., Nagar, N. M., Falcke, H., Wilson, A. S. 2005, ApJ, 625, 699
- Meurer, G. R., Heckman & T., Calzetti, D. 1999, ApJ, 521, 64
- Nagar, N. M., Falcke, H., Wilson, A. S., Ho, L. C. 2000, ApJ, 542, 186
- Nagar, N. M., Falcke, H., Wilson, A. S. 2005, A&A, 435, 521
- Netzer, H. 2009, MNRAS, 399, 1907
- Reddy, N. A., Steidel, C. C., Fadda, D., Yan, L., Pettini, M., Shapley, A. E., Erb, D. K., & Adelberger, K. L. 2006, ApJ, 644, 792
- Rigopoulou, D. et al. 2000, ApJ, 537, L85
- Salim, L. et al. 2007, ApJS, 173, 267
- Sanders, D. B. & Mirabel, I. F. 1996, ARA&A, 34, 749
- Sargsyan, L., Weedman, D. W. 2009, ApJ, 701, 1398
- Seibert, M. et al. 2005, ApJ, 619, 55
- Sternberg, A. 1998, ApJ, 506, 721S
- Sternberg, A., Hoffmann, T. L., Pauldrach, A. W. A. 2003, ApJ, 599, 1333S
- Sturm, E. et al. 2006, ApJ, 653L, 13S
- Symeonidis, M., Willner, S. P., Rigopoulou, D., Huang, J.-S., Fazio, G. G., Jarvis, M. J. 2008, MNRAS, 385, 1015
- Veilleux, S., Kim, D. C., Sanders, D. B., Mazzarella, J. M., Soifer, B. T. 1995, ApJS, 98, 171V
- Villar, V., Gallego, J., Prez-Gonzalez, P. G., Pascual, S., Noeske, K., Koo, D. C., Barro, G., Zamorano, J. 2008, ApJ, 677, 169V
- Villar, V., Gallego, J., Prez-Gonzalez, P.-G., Barro, G., Zamorano, J., Noeske, K. G., Koo, D. C. 2011, arXiv1107.4371V
- Wuyts, S. et al. 2011, ApJ, 738, 106, 5502W
- Zhao, Y., Gu, Q., Gao, Y. 2011, AJ, 141, 68